JOM
https://doi.org/10.1007/s11837-024-06717-w

A Review of Cluster Dynamics in Studying Radiation Damage: Dominant Factors and Practical Implications

YAOXU XIONG,[1] SHASHA HUANG,[1] JUN ZHANG,[1] SHIHUA MA,[1] BIAO XU,[1] HAIJUN FU,[1] XUEPENG XIANG,[1] WENYU LU,[1] and SHIJUN ZHAO[1,2,3]

1.—Department of Mechanical Engineering, City University of Hong Kong, Hong Kong, China. 2.—Shenzhen Research Institute of City University of Hong Kong, Shenzhen, China. 3.—e-mail: shijzhao@cityu.edu.hk

Radiation damage to structural materials is a pivotal concern impacting the safety and stability of nuclear energy systems. The microstructure alterations induced by irradiation encompass defect generation, diffusion, and interaction over extended durations. Cluster dynamics (CD), a mesoscopic simulation method, has proved instrumental in studying the protracted evolution of microstructures. By solving the master equations that describe a series of cluster growth processes in CD models, we can facilitate the computation of physical quantities, including defect cluster size, number density, and volume fraction, thereby unveiling the mechanism governing cluster evolution. Stimulated by recently renewed interest in mesoscale simulations, this review examines critical factors in CD, such as cluster mobility, intra-cascade cluster formation, temperature, and radiation conditions, shedding light on their significant roles in shaping long-term cluster evolution. Furthermore, the application of CD models in modeling different irradiation effects on nuclear materials is expounded, encompassing irradiation-induced cluster nucleation and growth, precipitation, and swelling. Finally, we provide a summary of the limitations inherent in CD models and outline prospects for enhancing their effectiveness in elucidating the evolution mechanism of microstructures under irradiation conditions.

INTRODUCTION

Nuclear energy has emerged as a clean and economically reliable source of baseload power over the past five decades, serving as a pivotal solution to both energy demand and environmental concerns.[1,2] The operational environments within nuclear reactor cores are exceptionally harsh, characterized by extreme temperatures, pressures, and intense radiation flux. Consequently, structural materials deployed in these reactors must possess exceptional resilience to endure substantial irradiation-induced microstructural changes. The magnitude of irradiation-induced damage is commonly quantified through displacement per atom (dpa), reflecting the average number of displaced atoms per atom in a material resulting from irradiation. Throughout the operational lifespan of nuclear reactors, materials can accumulate irradiation doses reaching hundreds of dpa, leading to a huge number of irradiation defects, which threaten the performance of reactor components on an engineering scale. The capacity of materials to withstand radiation-induced damage ultimately hinges upon defect evolution in irradiated materials. Thus, gaining insight into the mechanisms underlying microstructural damage caused by irradiation holds profound implications for the design of irradiation-tolerant materials.[3–6]

Under irradiation, microstructure evolution is controlled by multiple processes, including defect accumulation, transportation, elimination and mutual interaction, and interaction with the existing microstructures. Unfortunately, it is difficult to

(Received April 11, 2024; accepted June 10, 2024)

Published online: 10 July 2024

clarify the micro-mechanism of defect evolution from experiments[7,8] due to the complex relationship between the evolution of defect population and irradiation conditions. Therefore, developing relevant theoretical simulation methodology is essential and irreplaceable.[9,10] Indeed, there is increasing research interest in simulations to reveal the atomic-scale processes involved in radiation damage and to understand the evolution of defects throughout the lifetime of materials in reactors.[11–16]

Because of the diverse time and length scales involved in radiation damage processes, it is necessary to employ approaches from multiple scales concurrently or sequentially to comprehensively describe the entire process. Electronic structure calculations based on density functional theory and atomistic molecular dynamics (MD) typically describe atomic-scale defect properties. Their direct comparison with experiments is challenging due to limitations in experimental characterization resolution. The cluster dynamics (CD) method offers a mesoscopic-scale description of physical phenomena, providing relevant information concerning the long-term dynamic evolution of defects in various materials.[17–19] The CD model characterizes the system as clusters that grow and dissociate by absorbing and emitting sub-clusters through numerical integration of kinetic equations governing defect accumulation, transportation, and elimination. The results, ranging from nano-sized defect clustering to large second-phase particle coarsening, directly influence the mechanical properties of materials and can be compared with experimental observations from advanced microscopes, thereby serving as a unique bridge connecting atomic-scale and macroscopic defect properties.[20–22]

The applications and challenges of CD in modeling defect evolution have been discussed in several review articles.[23–26] For instance, Kohnert et al.[23] highlighted the connection between CD modeling and traditional mean field rate theories, with a focus on challenges stemming from parameter uncertainty in CD modeling. They also proposed directions for using CD in developing combined models with other techniques such as crystal plasticity constitutive modeling. Chen et al.[24] explored differences in the CD model from algorithmic and computer implementation perspectives, comparing deterministic methods (such as the group method and the Fokker–Planck method or their combinations) with stochastic methods. They pointed out that, since the CD model consists of a set of coupled and stiff ordinary differential equations (ODEs), and the number of ODEs increases exponentially with defect size, efficiently solving a large number of ODEs is a major challenge. Zheng et al.[25] provided an overview of CD models, algorithms, and recent research progress. They specifically introduced the application of CD models to two typical issues: neutron irradiation effects and grain boundary radiation resistance in nuclear materials. Ke et al.[26] summarized different microstructure modeling tools for nuclear materials, including rate theories, CD, phase-field models, and kinetic Monte Carlo simulations. They compared the strengths and limitations of these methods and discussed currently available open-source tools, emphasizing the severe lack of empirical thermodynamic and kinetic data at the service condition temperatures (300–600°C) and the unexplored role of excess point defects in affecting phase stability. Most of these reviews focused on methodological development, with comparatively less emphasis on the characteristics of materials and irradiation conditions. The recent emergence of innovative structural materials, such as high-entropy alloys (HEAs) featuring multiple principal elements in roughly equal proportions, has inspired renewed interest in CD modeling for predicting defect evolution. In these alloys, the formation and migration of defect clusters are profoundly influenced by pronounced chemical disorder, leading to delayed and heterogeneous defect evolution. Consequently, there is a strong demand for long-term CD modeling techniques to elucidate how the composition and physical parameters of the material, as well as irradiation conditions, affect defect evolution.

CD modeling has been extensively applied to various types of materials commonly used in nuclear engineering. These materials include austenitic stainless steel for pressurized water reactors, low activation ferritic/martensitic steel as a candidate material for fusion reactors, Fe-based and Ni-based alloys as nuclear structural materials, tungsten alloys as plasma-facing components of fusion reactors, and nuclear fuel materials. In this context, we reexamine the application of CD simulations for long-term radiation damage simulation in these materials. We begin by introducing the master equation in CD simulations and discussing the critical factors affecting the modeling results. Subsequently, we review the application of the CD model in simulating various irradiation effects on the materials, including irradiation-induced dislocation loop formation, void and bubble nucleation and growth, irradiation-induced precipitations, and swelling. Specifically, we consider the movement modes of different types of clusters, as well as spatially varied defect diffusion influenced by its position and concentration, inhomogeneous defect implantation, and free surfaces. Finally, we discuss the challenges and future development of CD models as an effective approach to predicting long-term defect evolution in materials. This includes the need

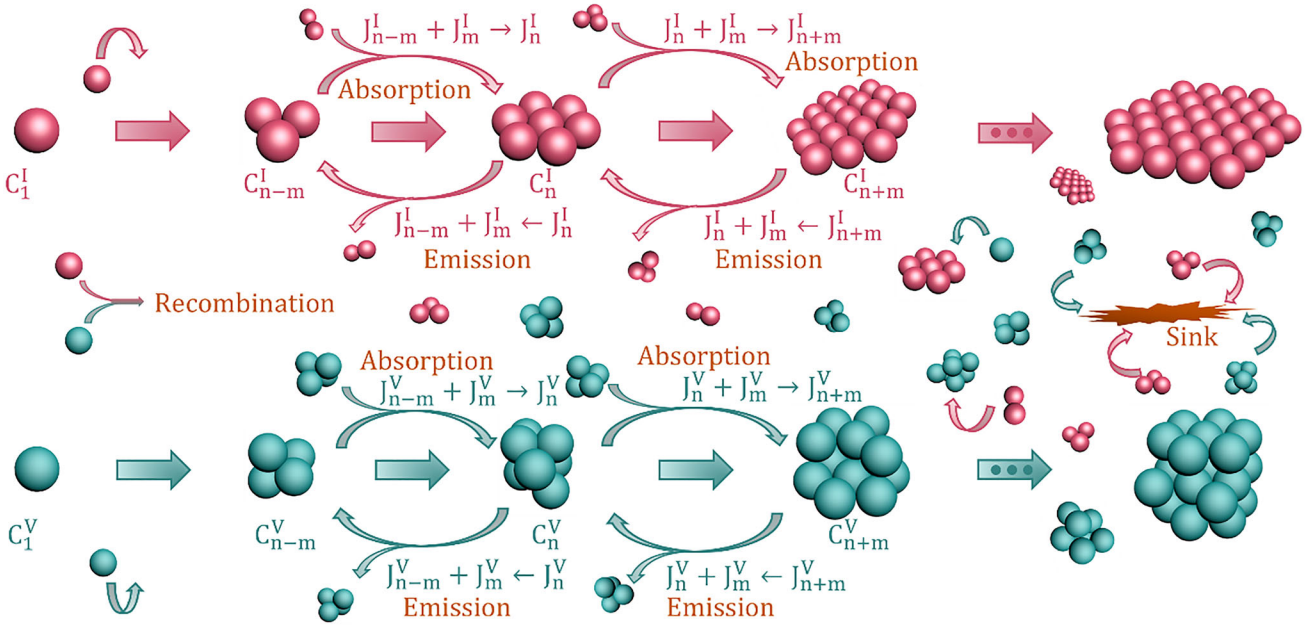

Fig. 1. Schematic of cluster transformation considered in the cluster dynamics model.

for accurate empirical data, the handling of complex defect interactions, and the integration of CD models with other simulation techniques to enhance predictive capabilities.

FUNDAMENTALS OF CLUSTER DYNAMICS

In CD models, the evolution of defect clusters is depicted as a sequence of chemical reactions that describe the changes in concentration. This approach is useful for delineating the nucleation, growth, and coarsening processes of defect clusters, as illustrated in Fig. 1. Clusters undergo enlargement by absorbing defects and diminish in size by emitting defects. In the context of the CD model, defects encompass interstitials, vacancies, and their corresponding clusters, while monomers refer to single interstitials and vacancies.

Homogeneous Cluster Dynamics

For the homogeneous cluster dynamic, all monomers are assumed to be equivalent, obviating the need to distinguish between monomers situated at nucleation positions. The time evolution of the concentrations of these defects is described by a set of ordinary differential equations involving the number density of clusters (C_n) containing n atoms.[27–30]

Mobile clusters refer to clusters that are mobile and can be consumed by other defects. For mobile clusters up to a size of n_{max}, the master equation of CD that gives the time evolution of concentrations of clusters with different sizes C_n is written as:[19,20,27,31–36]

$$\frac{dC_{n,I}}{dt} = G_{n,I} + \sum_{m=1}^{\min(n-1,n_{max})} J_{I_{n-m}\rightarrow I_n} - \sum_{m=1}^{n_{max}} J_{I_n\rightarrow I_{n+m}} - \sum_{m\geq 1} J_{I_m\rightarrow I_{m+n}} - \frac{4\pi(R_{n,I}+R_{n,V}+d)(D_{m,I}C_{m,I}+D_{m,V}C_{m,V})}{\Omega} - D_{n,I}k_{n,I}C_{n,I}, \quad (1)$$

$$\frac{dC_{n,V}}{dt} = G_{n,V} + \sum_{m=1}^{\min(n-1,n_{max})} J_{V_{n-m}\rightarrow V_n} - \sum_{m=1}^{n_{max}} J_{V_n\rightarrow V_{n+m}} - \sum_{m\geq 1} J_{V_m\rightarrow V_{m+n}} - \frac{4\pi(R_{n,I}+R_{n,V}+d)(D_{m,I}C_{m,I}+D_{m,V}C_{m,V})}{\Omega} - D_{n,V}k_{n,V}C_{n,V}, \quad (2)$$

where the terms $\frac{dC_{n,I}}{dt}$ in Eq. 1 represent the concentration change rates of interstitial clusters with a size of n. The first item ($G_{n,I}$) on the right side of Eq. 1 denotes the generation rate of interstitial clusters with a size of n, and the second item describes the total cluster flux from the interstitial cluster of size $n-m$ to the cluster of size n. These two items contribute to the production of interstitial clusters with a size of n. The third and fourth items represent the total flux to form the clusters of size $n+m$ from a cluster of size n. The fifth item

represents the annihilation between interstitial and vacancy clusters. The sixth item signifies the absorption of a defect by the sink. Collectively, the third to sixth items account for cluster consumption. These master equations are applicable to interstitial-type dislocation loop growth, He bubble growth, and precipitation. Similarly, Eq. 2 follows a similar structure but pertains to vacancy clusters.

In the above equations, $J_{I_{n-m}\to I_n}$ denotes the total interstitial cluster flux from the cluster of size $n-m$ to the cluster of n. Considering interactions with both interstitials and vacancies,[34] it can be expressed as:

$$J_{I_{n-m}\to I_n} = \beta_{n-m,m,I}C_{n-m,I} - \alpha_{n,m,I}C_{n,I} - \beta_{n,m,V}C_{n,I} + \alpha_{n-m,m,V}C_{n-m,I}, \quad (3)$$

where the absorption coefficient $\beta_{n-m,m,I}$ for interstitials represents the rate at which a cluster with size of $n-m$ absorbs a mobile cluster of size m to form a cluster of size n. Similarly, the emission coefficient $\alpha_{n,m,I}$ signifies the process wherein a cluster with a size of n emits a mobile cluster of size m, leading to degradation to a cluster of size $n-m$. Analogously, $\beta_{n,m,V}$ and $\alpha_{n-m,m,V}$ denote the absorption and emission coefficients for vacancy clusters with the size of m, respectively.

For clusters, it is generally regarded that small dislocation loops formed by interstitials migrate one-dimensionally along the close-packed row of atoms in the lattice with migration energies less than 0.1 eV.[17] In contrast, vacancy-type defects exhibit three-dimensional movement, referring to random movement in three-dimensional space when mobile.[17] In one-dimensional motion, a lower migration energy barrier is usually found, resulting in long-distance diffusion of defects. In contrast, three-dimensional motion involves a higher migration energy barrier, leading to localized diffusion. The absorption and emissions coefficients, which govern the reaction coefficient, are outlined in Table I.

R represents the cluster radius, D denotes the cluster diffusion coefficient, and C signifies the cluster concentration. The symbol $\sigma_{m,n}$ corresponds to the cross-section for interaction, and λ_m denotes the mean free path for one-dimensional diffusion. G stands for Gibbs free energy, ρ_{dl} represents the dislocation density, r_{dc} indicates the dislocation capture radius. d denotes the grain size. l signifies the thickness, and φ represents the angle between loop mobility trajectory and surface normal. Further details on these parameters can be found in the literature[17,37,38]

The formulation of the master equation can exhibit significant variability depending on several factors, including the number of defect types present in the system, the types of defects allowed to migrate, and the selected defect reactions of the model. As the number of defect species increases, the number of differential equations required to simulate mixed-species clusters grows exponentially. In addition, the complexity of the equations escalates with an increase in the number of migrating defects. Therefore, the CD method is commonly constrained to a small number of species and mobile defects. Typically, the largest cluster usually is limited to tens of nanometers (9500 interstitials produce a dislocation loop of 10 nm). To enhance computational efficiency, various approximations to the ordinary differential equation sets have been employed. These approximations may involve random sampling methods,[39] casting into the Fokker–Planck formulation,[36,40–43] or complex grouping schemes.[44,45] These strategies help to streamline the computational process while preserving the essential dynamics of the system.

Spatially Resolved Stochastic Cluster Dynamics

The master equations derived for defect evolution are assumed to be spatially homogeneous, which approximates an infinite medium. However, in heterogeneous systems, such as polycrystals and nano-structured materials, defect evolution can only be accurately captured through a spatially resolved approach. For the spatially resolved stochastic cluster dynamics (SRSCD), monomer diffusion is affected by their position and concentration, allowing the study of inhomogeneous defect implantation and the effects of free surfaces. Addressing defect evolution in heterogeneous systems involves considering defect diffusion under the concentration gradients.[46–48] The spatially resolved defect evolution can be expressed as:

$$\frac{dC_n}{dt} = \nabla(D_n\nabla C_n) + f_{(C_n,t)}, \quad (4)$$

Table I. Defect reaction coefficients in the homogeneous CD

	Three-dimensional (3D)	One-dimensional (1D)
Cluster absorption coefficient	$\frac{4\pi(R_{n-m,I}+R_{m,I}+R_d)D_{m,I}C_{m,I}}{\Omega}$	$\frac{2D_{m,I}\sigma_{m,n}}{\lambda_m}$
Cluster emissions coefficient	$\beta_{n-m,m,I}\exp\left(-\frac{\Delta G_{n-m}+\Delta G_m-\Delta G_n}{kT}\right)$	
Dislocation absorption coefficient	ρ_{dl}	$8r_{dc}\rho_{dl}^{\frac{3}{2}}$
Grain boundary absorption coefficient	$\frac{6}{d^2}$	$\frac{24}{d^2}$
Surface absorption coefficient	$\frac{2}{l^2}$	$\frac{8cos^2\varphi}{l^2}$

Table II. Reaction rate of various clustering and diffusion events used in the SRSCD

Reaction	Rate (s^{-1})
3D–3D clustering	$Z_{int}\left(\omega^{*}+\omega\left(n_i^{\frac{1}{3}}+n_j^{\frac{1}{3}}\right)\right)(D_iD_j)N_iN_j\frac{\Omega}{V}$
3D–1D clustering	$Z_{int}\left(\omega^{*}+\omega n_i^{\frac{1}{3}}+\omega\prime n_j^{\frac{1}{2}}\right)D_iN_iN_j\frac{\Omega}{V}+Z_{int}^{4}\left(\omega_{1D}^{*}+\omega_{1D}n_i^{\frac{1}{3}}+\omega_{1D}\prime n_j^{\frac{1}{2}}\right)^{4}D_jN_i^{2}N_j\left(\frac{\Omega}{V}\right)^{2}$
3D–3D clustering	$Z_{int}^{4}\left(\omega_{1D}^{*}+\omega_{1D}\prime\left(n_i^{\frac{1}{2}}+n_j^{\frac{1}{2}}\right)\right)^{4}\left(D_iN_j+D_jN_i\right)\left(\frac{\Omega}{V}\right)^{2}$
Dissociation	$\omega n_i^{\frac{4}{3}}D_ie^{-\frac{E_b(n_j)}{k_bT}}N_i$
Trapping at sinks	$Z_{int}\rho D_iN_i$
Diffusion	$\frac{D\Omega_{ij}\left(N_i-N_j\right)}{VL_{ij}}$

$\boldsymbol{Z_{int}}$ denotes the interstitial absorption bias factor, $\boldsymbol{\omega}$, $\boldsymbol{\omega^{*}}$, $\boldsymbol{\omega_{1D}^{*}}$, $\boldsymbol{\omega\prime}$, and $\boldsymbol{\omega_{1D}\prime}$ represent the reaction rates between 3D and 1D migrating circular and spherical defects, $\boldsymbol{n}$ denotes the size of the cluster, $\boldsymbol{D}$ represents the diffusion coefficient, $\boldsymbol{N}$ signifies the number of clusters, $\boldsymbol{\rho}$ denotes the dislocation density, $\boldsymbol{L}$ stands for the distance between the centers of the elements, Ω represents the atomic volume, and $\boldsymbol{V}$ indicates the finite volume of the elements in the SRSCD. Additional details regarding these parameters are available in the literature.[48,49]

where the first item represents defect diffusion, and the second item encompasses all the terms discussed in the previous section.

The determination of the pertinent reaction rates, including defect diffusion, defect creation, clustering, dissociation, annihilation, and trapping at sinks, stands as a pivotal component in SRSCD. These rates are detailed in Table II. Note that the one-dimensional diffusion of circular dislocation loops is explicitly taken into account in clustering rates.

In the context of SRSCD, materials such as thin films can be modeled by setting the defect concentration outside the materials equal to zero along one axis while applying periodic boundary conditions along the other two axes.[48] To solve the rate equations presented in SRSCD, reactions are first selected, and time is iterated in a stochastic manner, instead of using a standard finite-difference time iteration formulation as in the homogeneous CD. The stochastic approach in SRSCD is particularly advantageous when dealing with a high number of potential cluster configurations. In particular, it often outperforms deterministic methods in microstructure models that involves sink evolution with chemical segregation or precipitation, especially where the cluster space may involve two or more solute elements in addition to lattice defects. Another benefit of the stochastic method is its ability to sample a range of possible microstructural outcomes from a set of physical processes, thereby providing a statistical quantification of the potential experimental observations. Due to the stochastic nature of SRSCD, simulations using the same input parameters may exhibit significant variations, and most simulations are typically conducted multiple times to obtain the averaged result.

DOMINATING FACTORS INFLUENCING CD

The evolution of defects is governed by a complex interplay between kinetics and thermodynamics. Thermodynamic equilibrium analyses play a crucial role in predicting eventual outcomes, while kinetics, encompassing aspects like diffusion under different temperatures, are indispensable in understanding the mechanisms driving cluster growth. In this section, we delve into the primary factors influencing cluster evolution within the CD framework, shedding light on the intricate interplay between nucleation and growth mechanisms.

Cluster Mobility

In the CD model, if only single interstitials and vacancies are mobile, a cluster size of n occurs through the absorption of the monomer by the cluster size of $n-1$. In fact, clusters with the size of n can form by absorbing a series of mobile clusters, each no larger than n_{max}, given that clusters within the size of n_{max} exhibit mobility. As depicted in Eqs. 1 and 2, the total flux of C_n generated by this reaction is written as: $flux=\sum_{m=1}^{\min(n-1,n_{max})}J_{I_{n-m}\rightarrow I_n}$, which includes the flux of clusters of size less than or equal to n_{max} to form the C_n cluster. Here, the mobility of clusters significantly enhances their absorption coefficient, and such cluster mobility promotes their growth. For instance, while defect clusters in SiC have generally been assumed to be immobile due to their high migration barriers, recent experimental evidence suggests that clusters in SiC can undergo radiation-induced diffusion due to ballistic collision between incoming particles and cluster atoms under some irradiation conditions.[50] By considering this effect, Liu et al.[33] demonstrated that the mobility of clusters leads to an increase in

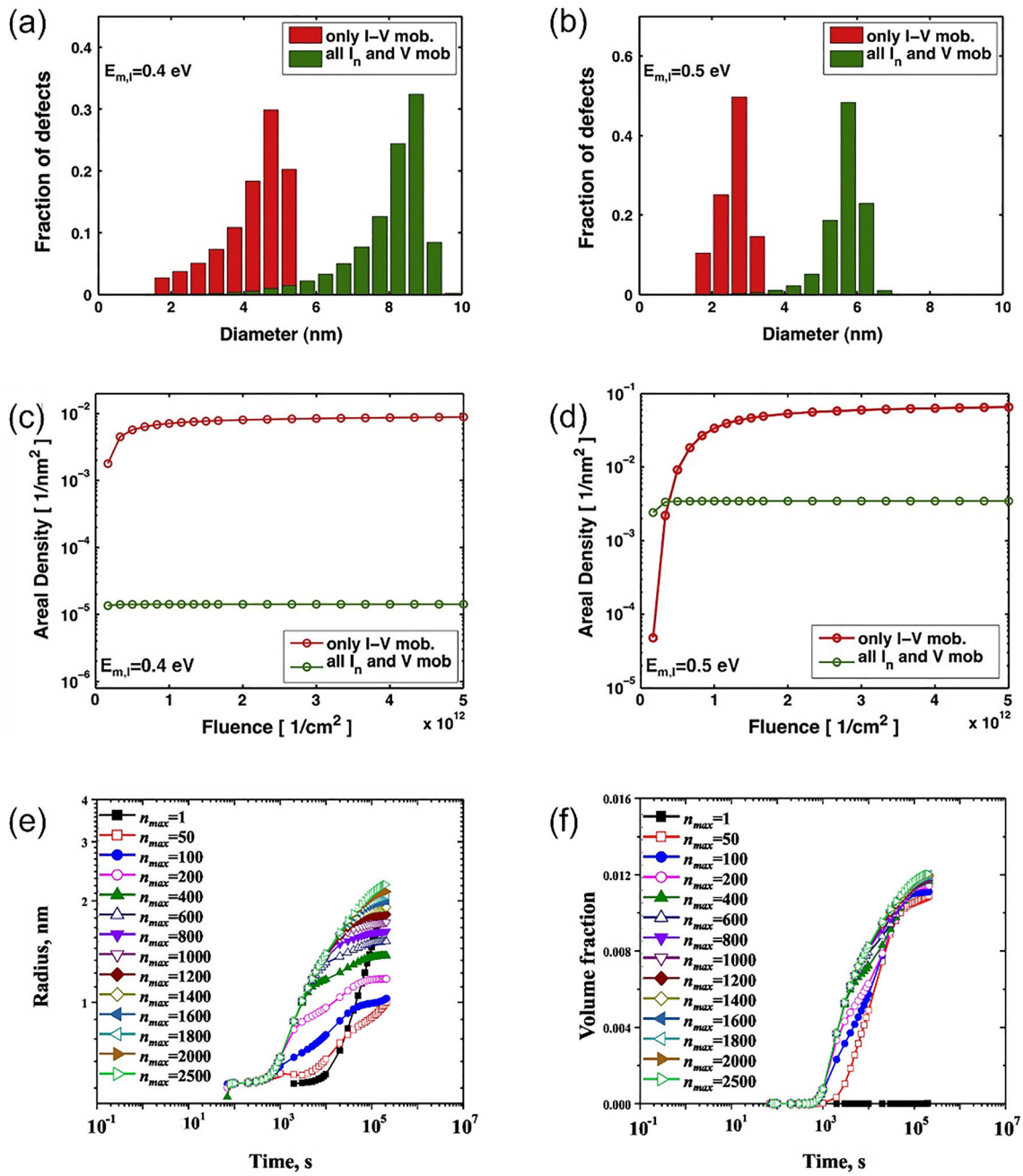

Fig. 2. Comparison of the size distribution after considering the mobility of clusters with (a) E_{mi} = 0.4 eV and (b) E_{mi} = 0.5 eV and their corresponding areal density (c, d); here, E_{mi} is the interstitial migration energy. Effect of n_{max} on the time evolution of the (e) mean radius and (f) number density of Cu clusters in Fe-Cu alloys. (a–d) Reprinted with permission from Ref. 51; (e, f) reprinted with permission from Ref. 52.

cluster size, enabling quantitative matching with large clusters in terms of dislocation loop diameter observed in experiments. In addition, Xu et al.[51] demonstrated that, compared with the case with immobile clusters, as shown in Fig. 2a–d, mobile clusters boost the cluster growth to a larger size and reduce the number density of clusters under varying irradiation fluences. This phenomenon is attributed to cluster mobilities which accelerate the cluster growth rate by capturing other mobile clusters at a faster pace, resulting in a significant reduction in their number density.

In investigations of copper precipitate evolution in FeCu alloys, Jourdan et al.[43] postulated that the effective diffusion coefficient of a single Cu interstitial is considerably greater than that of dimers, trimers, or larger clusters. It was found that ignoring the motion of clusters resulted in calculated cluster sizes that were smaller than those observed experimentally. In contrast, the kinetics of

cluster growth are accelerated by several orders of magnitude in the scenarios where the mobility of small clusters is considered. However, it remains uncertain to what extent mobile clusters can significantly influence the mean radius, number density, and volume fraction of Cu precipitates in Fe-Cu alloys. To address this uncertainty, Cui et al.[52] conducted an investigation where they varied the maximum size, n_{max} (ranging from 1 to 2500), of mobile clusters to examine its impact on the kinetics of Cu cluster precipitation in Fe-Cu alloy at 500°C, as demonstrated in Fig. 2e and f. The CD model reveals that introducing cluster mobility results in the initiation of cluster formation at an earlier time, compared to scenarios considering only the mobility of monomers. Specifically, the mean radius of Cu precipitates grows steeply and obeys $\overline{R} \propto t^{\frac{1}{2}}$ when only considering the mobility of monomers. In this condition, the calculated volume fraction and number density of precipitation are smaller compared to the experimental results. With the introduction of cluster mobility, Cu precipitates followed a growth law of $\overline{R} \propto t^{\frac{1}{3}}$, consistent with experimental observations.

Influence of Intra-Cascade Clusters

The generation term $G_{n,I}$ in the CD master equations. Eqs. 1 and 2. stems from intra-cascade cluster production which is directly formed during the damage collision stage.[53,54] This phenomenon was captured by transmission electron microscopy[50] and found necessary for CD models of iron[46,53,55] and molybdenum[51] to reproduce experimental cluster size distributions. Liu et al.[33] introduced the intra-cascade cluster production and scaled the distribution function to make sure the total number of interstitials in all the intra-cascade interstitial clusters matched the total production of interstitials in SiC. The resulting cluster size distribution from the CD model demonstrated a good agreement with experiments, as shown in Fig. 3a and b. In contrast, if the intra-cascade clusters are not considered, most of the clusters in CD simulations are larger than 1 nm, which is far beyond experiments as even the cascade efficiencies characterizing the effectiveness of atom displacement with respect to the Norgett–Robinson–Torrens standard vary from 0.001 to 1.0. This result demonstrates that the nucleation of clusters is suppressed due to the lack of intra-cascade clusters acting as nucleation sites. Introducing intra-cascade cluster production can bring down the peak cluster size because nucleation sites introduced by the intra-cascade effectively increase the nucleation rate of the cluster, resulting in a shift in the size distribution of clusters to a smaller size.

The intra-cascade cluster production can be captured by MD simulations. In recent studies, the MD-obtained cluster distributions in the cascade stage, which refers to the state immediately after the termination of high-energy particle bombardment, were fed into the CD model to examine the growth and evolution of clusters over long terms.[56,57] To elucidate the impact of the nucleation rate induced by intra-cascade clusters, different generation terms of small-sized clusters were investigated in Ni and NiFe.[57] The generation term of the small-sized cluster is denoted as $G_n = A \times n^{-B}$, where the concentration of small-sized cluster rises as B decreases, indicating a higher proportion of small-sized cluster formation. As depicted in Fig. 3c and d, the cluster distribution shifts leftward with the increase of small-sized cluster formation. The CD model brings to light that the smaller-sized cluster formation in the collision stage helps to increase the number density of clusters smaller than 2 nm and the higher nucleation rate inhibits the growth of clusters.

Materials Compositions

It has been observed that variations in material compositions can lead to significant alterations in the evolution of defects, thereby influencing the overall behavior and properties of materials. Indeed, the intrinsic properties of materials exert a profound influence on the behavior of defects, primarily through their composition and the environment surrounding the defects. These intrinsic properties dictate various phenomena, such as defect migration, reorganization, and the absorption and emission of clusters within the material. These processes play pivotal roles in governing the nucleation and growth rates within the CD model.[20,58] The absorption coefficient, $\alpha_{n-m,m} = \frac{4\pi(R_{n-m}+R_m+R_d)D_m C_m}{\Omega}$, highlights that lower migration energies facilitate cluster diffusion, enhancing cluster growth. For example, Xiong et al.[56] revealed that, even though the cluster size distribution is similar in VTaTi and VTaW in the primary damage state, the different cluster migration energies have a remarkable impact on the kinetic growth process. Compared to VTaW, the higher migration energy in VTaTi leads to a smaller growth rate, resulting in a smaller characteristic size of clusters in VTaTi under different radiation doses. Coefficients describing the absorption rate in the system containing precipitation components are given by $\omega^{(+)}_{n,n+1} = 4\pi c_\beta r_\alpha \sum_{i=1}^{k} \left(\frac{\upsilon_{i\alpha}^2}{x_{i\beta} D_i}\right)^{-1} n^{1/3}$, where c_β represents the total volume concentration of particles of different components in the phase, and r_α is the atomic radius of each precipitating phase. Parameter $x_{i\beta}$ accounts for the mole fraction of the different components, and $\upsilon_{i\alpha}$ denotes the change in the composition of component i as the cluster grows from size of n to $n+1$. Mamivand et al.[19] found that increasing Cu content accelerated the formation of Cu-MnNiSi precipitation. As demonstrated in Fig. 4a and b, the presence of 0.05 at.% Cu is shown to expedite precipitation and shift the upswing in Cu-

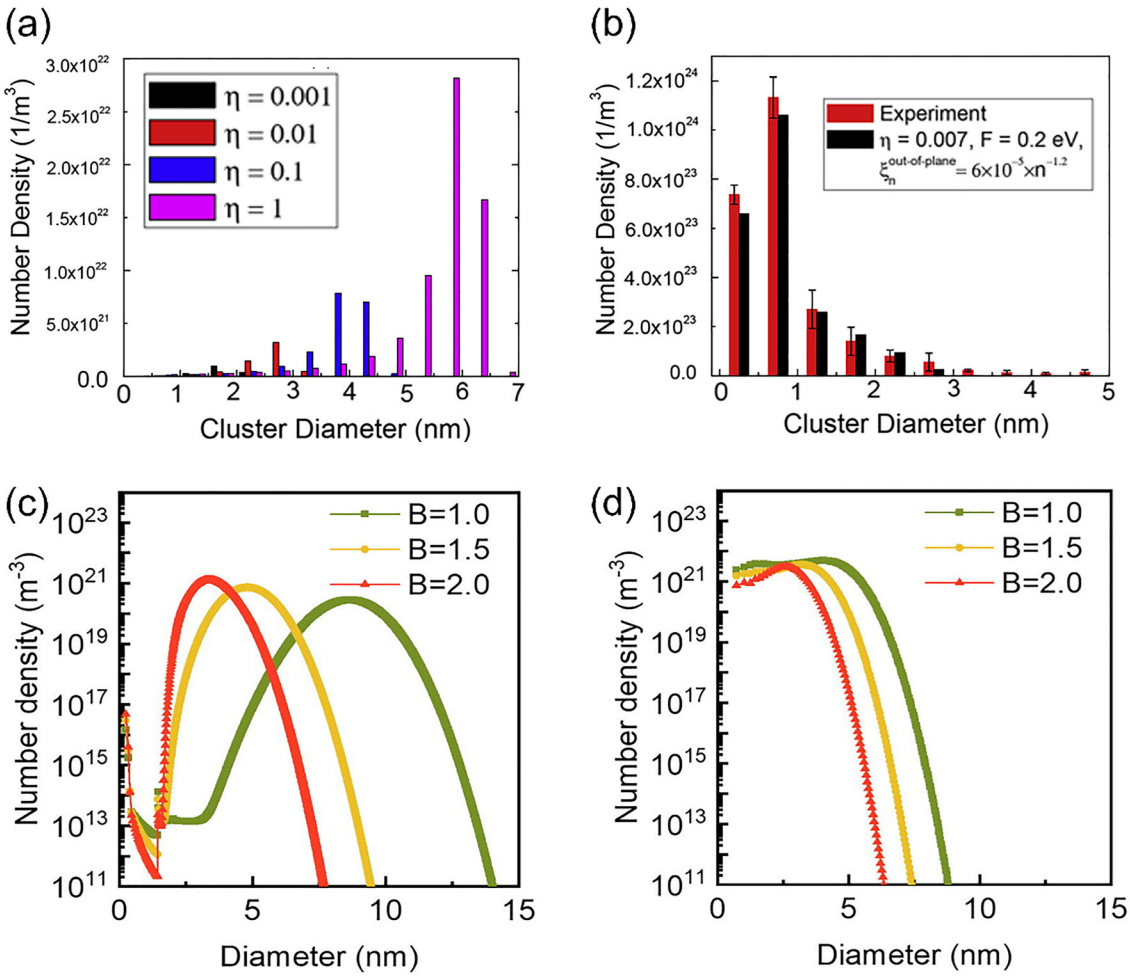

Fig. 3. (a) Cluster size distribution from the CD model with different cascade efficiencies η in SiC. (b) Comparison of the cluster size distribution between the experiment and the CD model. (c, d) Cluster size distribution at the different intra-cascade ratios in Ni and NiFe, respectively. Intra-cascade-induced generation term of small-sized cluster distribution is denoted as $G_n = A \times n^{-B}$. (a, b) Reprinted with permission from Ref. 33; (c, d) reprinted from Ref. 57 under Creative Commons License CC-BY.

MnNiSi formation to lower fluence. Notably, the diffusion coefficient of Cu is significantly higher than that of MnNiSi, facilitating the rapid formation of Cu-MnNiSi precipitation. Therefore, the higher content ($x_{i\beta}$) of Cu enhance the absorption of cluster and promotes the growth of Cu-MnNiSi precipitation.

The Gibbs free formation energy serves as a critical determinant of cluster stability. This parameter essentially dictates the likelihood of nucleation events occurring within the material. For instance, Briggs et al.[59] hypothesized that the larger radiation-induced cluster observed in Ni-5Cr compared to Ni-18Cr alloys was attributed to the lower Gibbs free energy of clusters. Indeed, ab initio calculations indicate strong binding between Cr and interstitials in Ni-Cr alloys; a 10 wt.% increase in Cr concentration would increase the binding energy by approximately 0.1 eV. Correspondingly, in the CD model, different binding energies (E_{b2i}), 0.73 eV for Ni-5Cr and 0.9 eV for Ni-18Cr, were used as input parameters for Ni-5Cr and Ni-18Cr. The simulated results align with experimental findings regarding both the size distribution and number density as shown in Fig. 4c and d. Therefore, the increased concentration of Cr is expected to enhance cluster nucleation, thus leading to a decrease in the average cluster size. However, it should be noted that, in the case of the Ni-18Cr alloy, the CD model functions more as a qualitative tool than a quantitative one. This limitation may arise from the fact that the model only considers the E_{b2i} parameter for the two alloys, eliminating the impact of changes in Cr concentration on defect migration.

Temperature

Temperature serves as a pivotal parameter dictating the evolution of defect clusters within materials. According to the Arrhenius relationship, the cluster diffusivity is closely related to temperature, and the variation in temperature affects the absorption and emission coefficients in CD models. Research conducted by Brimbal et al.[60] exemplified the impact of temperature on the microstructural

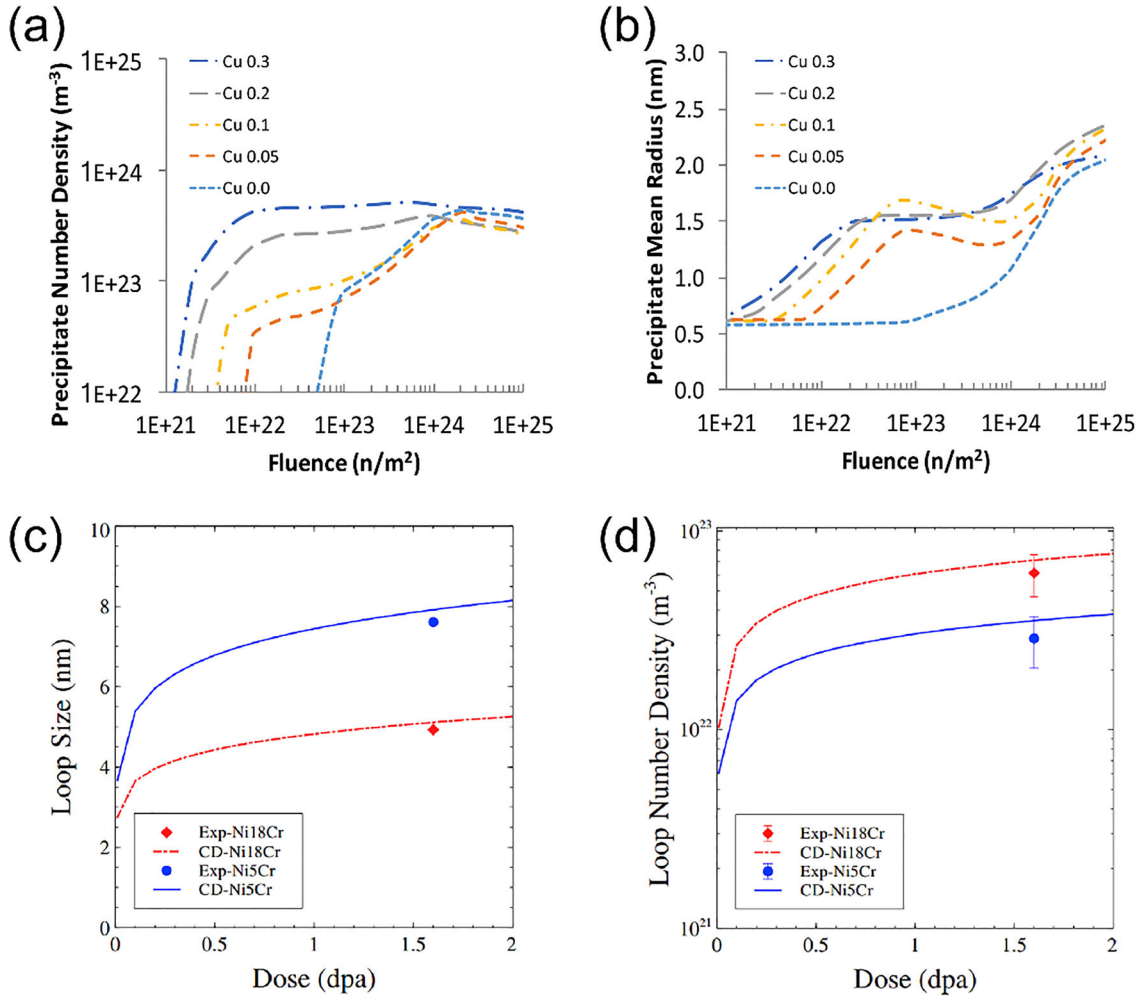

Fig. 4. (a) Number density and (b) mean radius of Cu-MnNiSi precipitation in reactor pressure vessel steel for a medium solute alloy under different fluence with various Cu content (at.%) at 290°C. (c) Loop size and (d) number density evolution for Ni-5Cr and Ni-18Cr at 400°C under proton irradiation. (a, b) Reprinted with permission from Ref. 19; (c, d) reprinted with permission from Ref. 59.

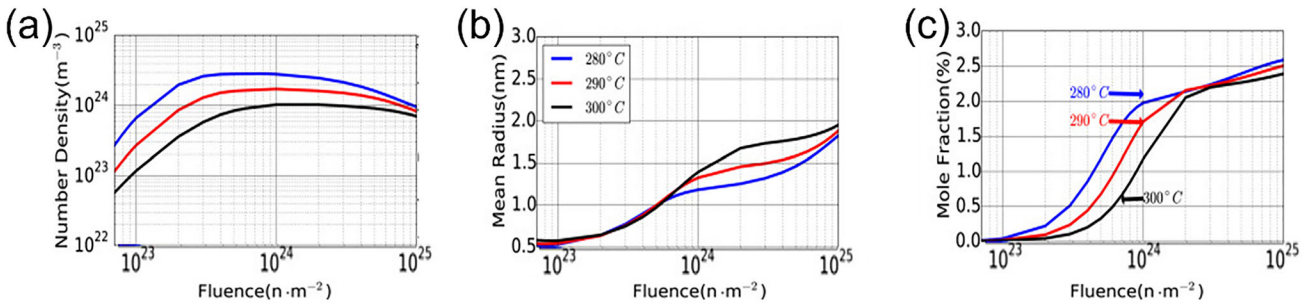

Fig. 5. The effect of temperature on the evolution of Mn-Ni-Si precipitates for (a) number density, (b) mean radius, and (c) mole fraction in Fe−1.45 at.%Mn-1.65%Ni-0.45%Si. Reprinted with permission from Ref. 27.

evolution of austenitic steels subjected to helium irradiation through CD. Simulation results have shown that the size of the cavity increases with rising temperature, attributed to enhanced reaction rates facilitated by temperature elevation. Furthermore, the evolution of Mn-Ni-Si precipitates in steels is shown to be sensitive to the irradiation temperature,[27] as illustrated in Fig. 5. In alloys with a composition of 1.45 at.%Mn-1.65%Ni-0.45%Si steels, an increase in temperature leads to a decrease in both the number density of clusters and their mole fraction, while the mean radius exhibits an upward trend with increasing temperature. Indeed, observations of increased cluster

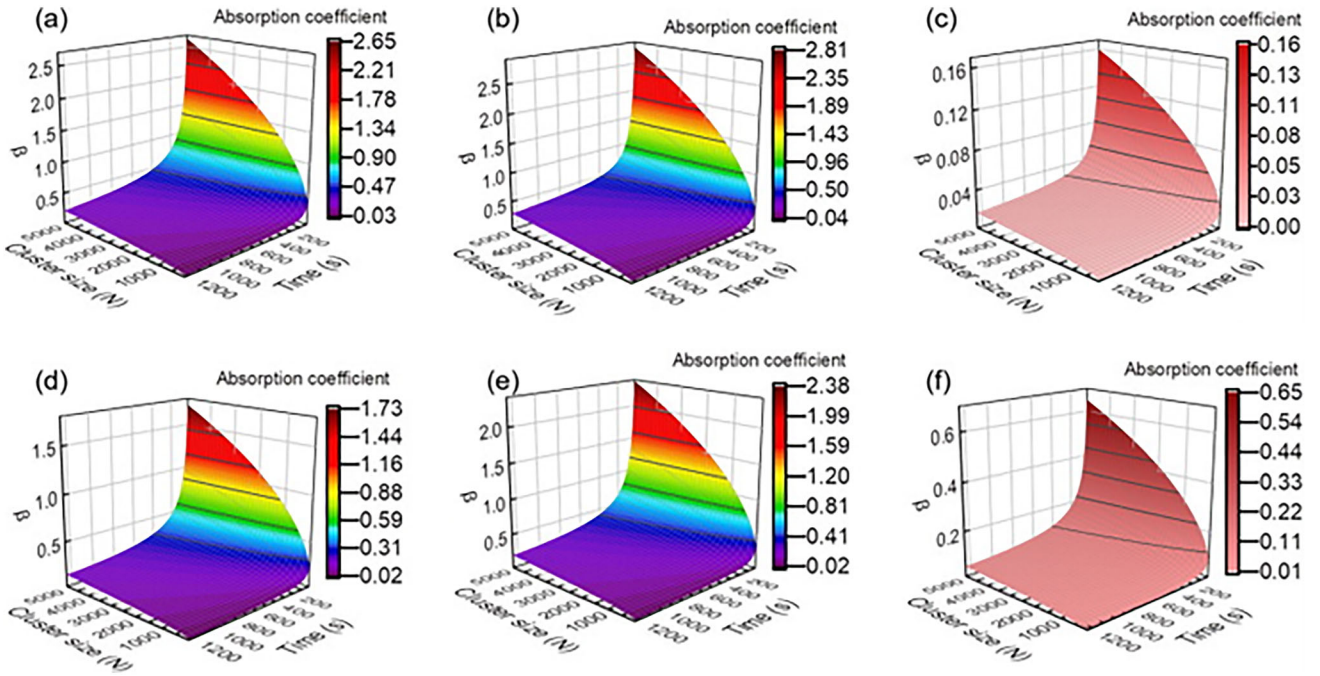

Fig. 6. The effect of temperature on the absorption coefficient. (a, b) The absorption coefficient of clusters in Ni at 300 and 400 K, respectively. (c) The difference between (a) and (b). (d, e) The absorption coefficient of clusters in NiFe at 300 and 400 K, respectively. (f) The difference between (d) and (e). Reprinted with permission from Ref. 57 under Creative Commons License CC-BY.

reaction rates with rising temperatures have been consistent across various simulations and experimental investigations.[37,61,62] However, it is worth noting that such a trend related to temperature can vary significantly across different materials due to the sensitivity of defect evolution in various materials to temperature variations.

To quantify the effect of temperature on cluster evolution, Xiong et al.[57] explored the size distribution of clusters across a temperature range from 200 K to 500 K. The CD results revealed a consistent trend: the averaged size of clusters in both Ni and NiFe alloys increases progressively with rising temperatures. However, a notable distinction emerges regarding the sensitivity of cluster size distribution to temperature changes, particularly in NiFe. Figure 6 shows the absorption coefficients of clusters of different sizes in Ni and NiFe at 300 K and 400 K, respectively. Notably, the absorption coefficients of Ni clusters exhibit minimal variation across different temperatures. In contrast, the absorption coefficients of NiFe clusters display a substantial variance, with differences as high as 0.65. The response of cluster absorption capacity to different temperatures is not consistent across different materials, indicating the complexity of temperature effects in cluster evolution. These findings highlight the critical role of material-specific characteristics, such as migration energy barriers, in determining cluster absorption coefficients at various temperatures. In the case of Ni, characterized by a low migration energy of 0.16 eV, irradiation-induced defects exhibit considerable mobility. Consequently, the modest increase in temperature from 300 K to 400 K restricts the absorption coefficient enhancement for clusters. Conversely, for NiFe, with a higher migration energy of 0.56 eV, defect mobility is limited. As a result, the rise in temperature significantly amplifies the absorption coefficient of clusters.

Irradiation Conditions

Experiments consistently reveal that, under given irradiation conditions, the average size of clusters tends to increase with escalating irradiation dose.[63–65] This phenomenon is primarily ascribed to the heightened concentration of monomers and prolonged irradiation duration, which collectively drive the growth of clusters toward larger sizes. Pellegrino et al.[34] conducted an investigation into the response of ZrC to heavy ion irradiation at room temperature. Employing CD methods, they simulated the evolution of interstitial clusters at various fluences, from 10^{11} cm^{-2} to 10^{17} cm^{-2}. The results elucidate a noteworthy shift in the distribution of cluster sizes towards larger values with increasing ion fluence, as demonstrated in Fig. 7a.

While the ability to reach high doses within hours rather than over extended periods such as months or years would be advantageous, it is essential to recognize that differences in dose rates, related to the generation term (G_n), can profoundly influence the rate of implanted damage. Consequently, even under equivalent irradiation doses, significant

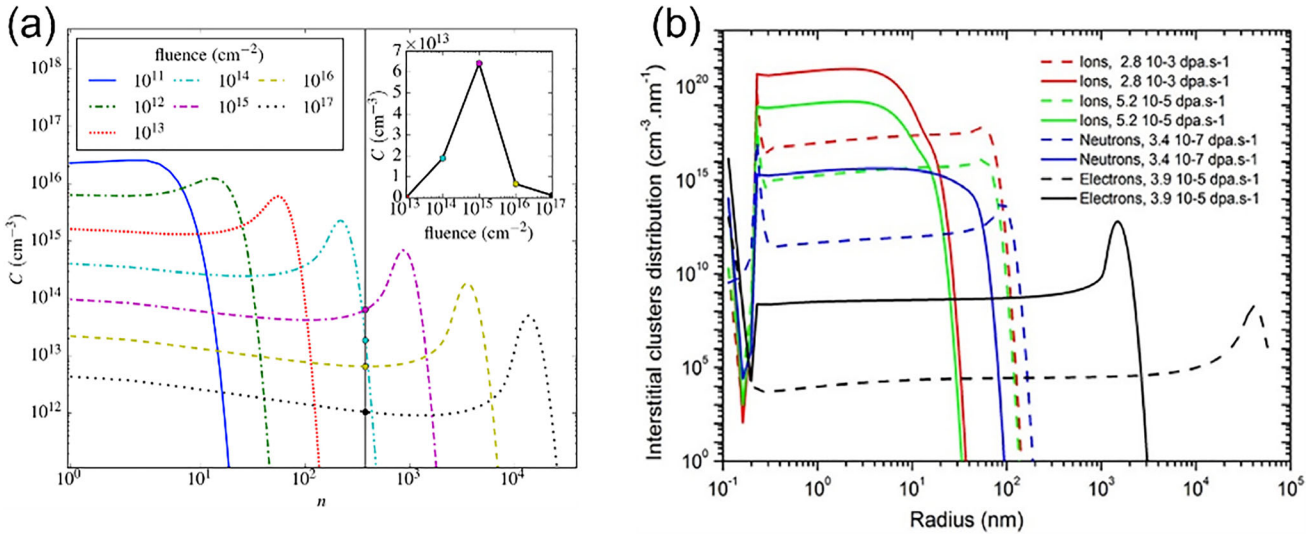

Fig. 7. (a) Cluster size distribution at different fluences. (b) Interstitial cluster size distribution obtained by the CD modeling at different dose rates. (a) Reprinted with permission from Ref. 34; (b) reprinted with permission from Ref. 70.

disparities can be found in cluster number density and size distribution,[66–68] arising from different energies of incident particles under various irradiation conditions. Gokhman et al.[69] utilized the CD model to simulate the formation of vacancy and self-interstitial clusters in pure Fe under varying doses of neutron irradiation. The results revealed a dramatic increase in the number density of interstitial-type clusters at low levels of neutron exposure. The density saturated when the neutron exposure exceeded approximately 0.025 dpa. The obtained averaged cluster diameter in the CD model and experiments is about 9 nm at 0.19 dpa. In contrast, heavy ions can deliver high levels of radiation damage faster than neutrons with a high dose rate. Gao et al.[17] used the CD model to explore the cluster size distribution in pure iron irradiated by Fe^+ ions, and both the experiment and CD results showed that the averaged cluster diameter is about 5 nm, which is smaller than the averaged cluster diameter of 9 nm in Fe exposed by neutron irradiation.[69] Further exploration by Soisson et al.[70] delved into the effects of different dose rates (electron, ion, and neutron irradiation) on the precipitation process in FeCr alloys using the CD model. Although the parameters controlling cluster behaviors, such as formation, migration, and binding energies, are similar, the fractions of n-sized clusters created by primary cascades vary under different radiation conditions. For instance, electron irradiation yields no clusters, while neutron irradiation produces n-sized interstitial clusters (f_n^i) and m-sized vacancy clusters (f_m^v), leading to the increased number density of small-size clusters (with a radius smaller than 0.5 nm). Compared with the cluster size distribution obtained by electron and neutron irradiations as demonstrated in Fig. 7b, the CD model reveals that a higher dose rate increases the number density but decreases the largest cluster size. This microstructural distinction underscores the significance of dose rate in modeling cluster evolution with CD, elucidating the constraints associated with substituting heavy ions and protons for expensive neutron irradiation when investigating the radiation tolerance of materials.

APPLICATION

The CD model seamlessly integrates the microscopic collision processes and defect growth dynamics with macroscopic microstructural changes. Within the realm of irradiation effects, the CD model has demonstrated remarkable efficacy in elucidating various phenomena, including the evolution of irradiation-induced defect clusters, precipitation, and void swelling. In the following section, we will introduce how the CD model is applied in the above scenarios.

Irradiation-Induced Defect Nucleation and Growth

The most straightforward application of CD is to describe the evolution and distribution of irradiation-induced defect clusters, since the solutions of CD equations explicitly provide the concentrations of clusters in different sizes under given conditions. The obtained cluster size distribution and number density form the cornerstone for analyzing microstructural changes and other related properties. Extensive investigations utilizing the CD model have been conducted across diverse materials, encompassing metals and alloys such as W,[71] Mo,[51] Fe and Fe alloys,[17,39,57,72,73] Zr and Zr alloys,[18,61,74–76] and ceramics.[33,34,77,78]

To investigate the dislocation loop evolution under the synergistic irradiation of He and neutron at 873 K in W, Li et al.[71] established a CD model to

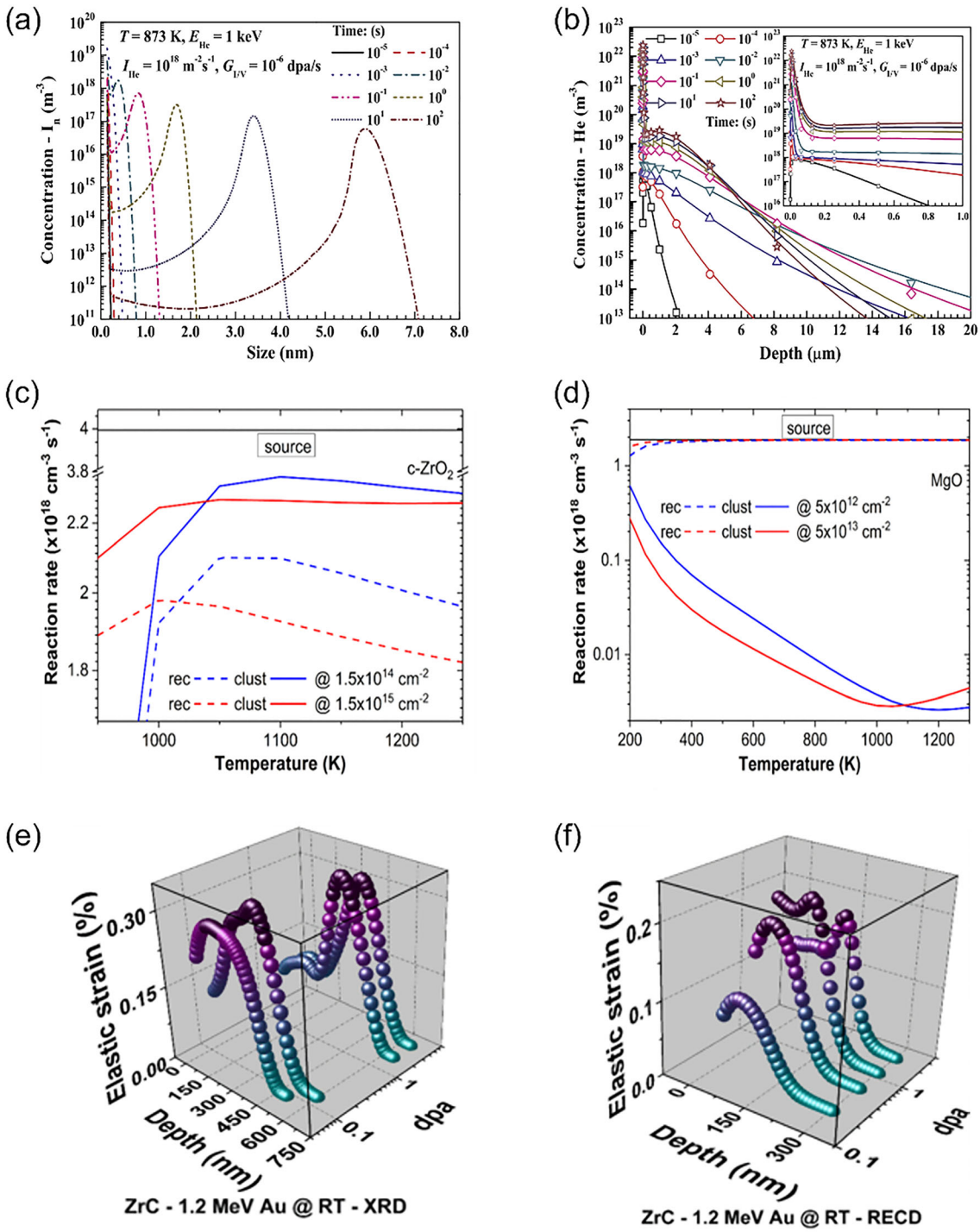

Fig. 8. (a) Evolution of interstitial cluster size distribution with time in tungsten. (b) Helium concentration distribution with depth under the synergistic irradiation of helium atom and neutron in tungsten. Reaction rate determined from CD simulations as a function of temperature for (c) c-ZrO_2 and (d) MgO. Elastic-strain depth profiles in ZrC obtained from (e) the experiment and (f) the CD model. (a, b) Reprinted with permission from Ref. 71; (c, d) reprinted with permission from Ref. 78; (e, f) reprinted with permission from Ref. 79.

explore the evolution of different types of defects, including self-interstitials, vacancies, helium atoms, and their clusters, over time. Figure 8a illustrates the evolution of interstitial cluster size distribution, revealing a sharp peak with the number density of approximately 10^{18} m^{-3} at the irradiation time of 0.01 s, followed by a shift towards larger cluster sizes over extended periods, aligning with experimental observations. In addition, the CD model incorporated a diffusion term, $D_\theta \nabla^2 C_\theta$, to show the depth distribution of helium concentration as depicted in Fig. 8b. The quantitative analysis of

concentrations and depth provides insights into the dynamic behavior of defects in plasma-facing materials. Similarly, Xu et al.[51] investigated defect evolution in nanometer-thick Mo foils subjected to 1 MeV krypton ion irradiation at 80°C, incorporating intra-cascade cluster production and spatial diffusion in their CD model. By setting the concentration of defects on the foil surface to zero in the diffusion term of $D_\theta \nabla^2 C_\theta$, the CD model elucidated the influence of foil thickness on defect evolution. Their findings revealed that interstitials in the foil center exhibited greater growth compared to those near the surface, forming larger loops. The averaged defect density in foils tended to become independent of thickness as the foil thickness increased from 12 nm to 84 nm, which was attributed to the fact that the surface, serving as a sink, was sensitive enough to affect the mobile cluster concentration over a depth of several nanometers.

In materials with hexagonal close-packed (HCP) structures, the formation of interstitial and vacancy-type loops, referred to as prismatic loops and basal loops, induces anisotropic dimensional changes characterized by the expansion along the a-axis.[18,74,76] Li et al.[61] developed a CD model by considering point defect clusters and interstitial and vacancy loop clusters, as well as the two different reaction rates on basal planes and prismatic planes, to reproduce the observed irradiation growth along a-axis. The reaction rate equations for interstitial and vacancy loops are: $\frac{dN^a_{il}}{dt} = \beta^i_{3i} C_i C_{3i}$ and $\frac{dN^c_{vl}}{dt} = \frac{G^{NRT}\varepsilon_v}{\pi r_4^2 |b^c|}(1 - N^c_{vl}/N^c_{max})$, where β represents the absorption coefficient, G^{NRT} denotes the standard dose rate in dpa/s, ε_v signifies the fraction of vacancies produced in vacancy clusters within one free cascade, and r signifies the radius of the loop. The last term $(1 - N^c_{vl}/N^c_{max})$ accounts for the overlap effect of the vacancy loops, with further detailed information available in the literature.[61] The obtained evolution of radiation-induced loop density and size faithfully replicates the observed irradiation growth stages, encompassing the growth rate along both the a- and c-axes. The CD modeling confirms the anisotropic growth of defects in the HCP structure by adjusting different dislocation loop reaction rates.

Cubic (yttria-stabilized) zirconia (c-ZrO_2) and magnesia (MgO) are two materials of significant interest owing to their potential applications in nuclear energy, including both fission and fusion. Despite both materials retaining their crystalline character without undergoing any phase changes, they exhibit contrasting patterns of defect accumulation under irradiation temperature. Specifically, while defect accumulation is accelerated in c-ZrO_2, it is retarded in MgO. Debelle et al.[78] utilized the CD model to illustrate the opposite cluster accumulation phenomenon, attributing to the difference in the mobility for both interstitials and vacancies in MgO and c-ZrO_2. The reaction rate calculated by CD, depicted in Fig. 8c and d, illustrates this distinction. In c-ZrO_2, where interstitials and vacancies exhibit similar mobility, defect growth (clustering) is favored over defect recombination, accelerating defect accumulation, while, in MgO, the relatively immobile vacancies compared to interstitials lead to dominant recombination rather than growth, resulting in a decrease in the growth rate with the temperature and retarded defect accumulation. The CD model highlights the different reaction rates stemming from variations in interstitial and vacancy migration energies in the continuous damage accumulation process.

Defect accumulation in irradiated materials can result in lattice elastic strain, which can be analyzed to glean essential information regarding defect concentration through X-ray diffraction. Debelle et al.[79] integrated X-ray diffraction measurements with CD simulation to investigate the strain build-up and relaxation processes induced by defects in ZrC single crystals irradiated with 1.2 Mev Au at various fluences. Within the framework of linear elasticity, the total strain is expressed as $\varepsilon = N_v V_v^{rel} + N_I \Omega$, where N_v and N_i denote vacancy and interstitial density, respectively, V_v^{rel} is the relaxation volume of a vacancy, and Ω is the atomic volume. As demonstrated in Fig. 8e and f, the maximum strain keeps on shifting to the greater depth with increasing dpa level. The elastic strain result obtained from the CD model quantified the experimentally observed relationship between strain and defect evolution as a function of irradiation depth.

In summary, the CD model serves as a crucial tool in understanding the process of defect evolution. It plays a pivotal role in elucidating the evolution of irradiation defects across materials at different temperatures owing to variations in defect migration energies. By adjusting the material composition, the CD model offers a means to probe the feasible way to suppress the growth of defect clusters induced by irradiation. Consequently, a thorough comprehension of the defect evolution mechanism unveiled through CD facilitates the design of radiation-resistant materials.

Irradiation-Induced Precipitate

The irradiation-induced precipitation phenomenon involves the formation of secondary phases resulting from the clustering of specific elements facilitated by defect flux. Given the close correlation between precipitation and cluster evolution, CD modeling proves instrumental in describing precipitation kinetics.[18,80,81] In a study by Bai et al.[66] focusing on Cu precipitation in reactor pressure vessel steels with low Cu concentrations typically below 0.1 at.%, a CD model based on the homogeneous nucleation mechanism was employed to investigate the Cu precipitation process under

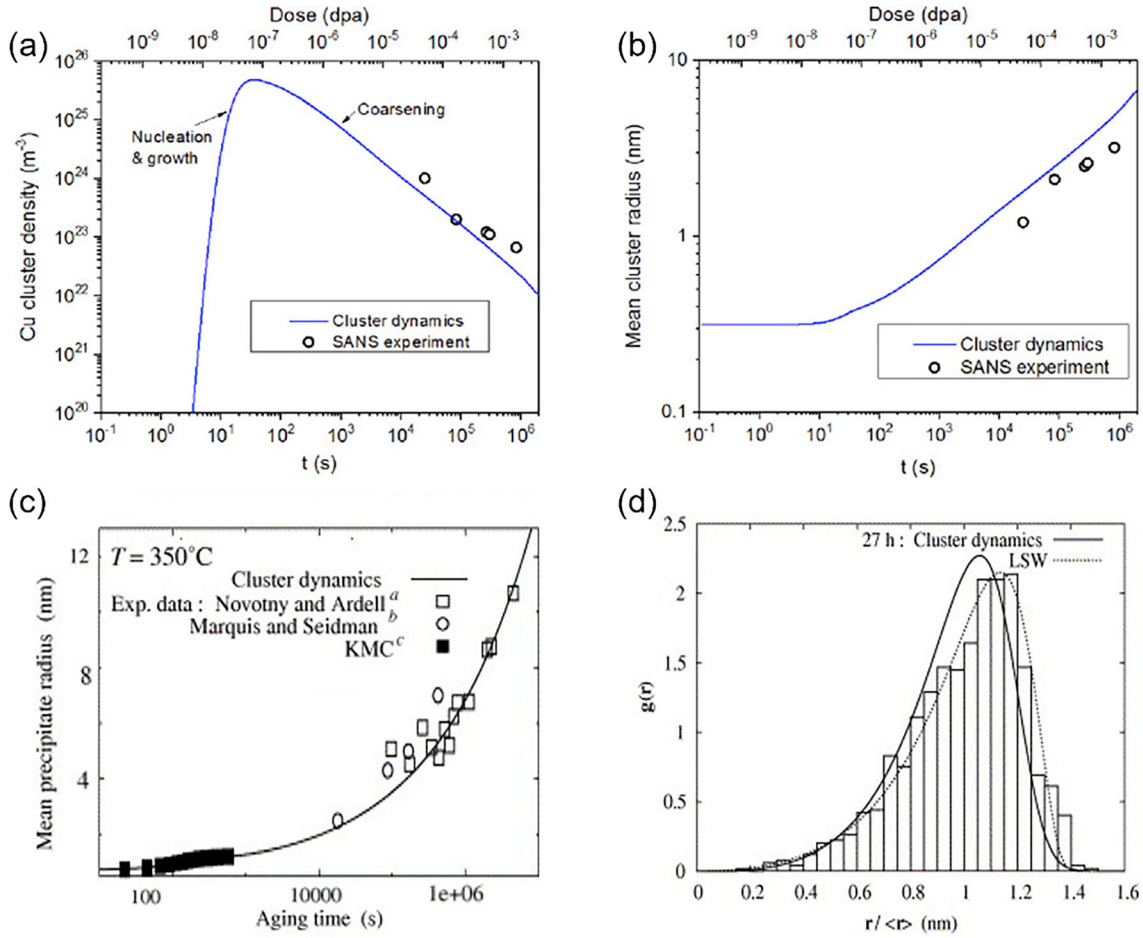

Fig. 9. (a) Number density and (b) mean radius of Cu precipitation as a function of time. (c) Mean precipitation radius and (d) precipitation size distribution compared with experimental results in the Al-Sc alloy. (a, b) Reprinted with permission from Ref. 66; (c, d) reprinted with permission from Ref. 83.

electron and neutron irradiation. Within the CD framework, when only Cu monomers are considered mobile and Cu clusters interact solely with single Cu atoms, the temporal evolution of the total number density of Cu clusters and the mean radius is shown in Fig. 9a and b. The initial phase, characterized by an increase in the total cluster number density and a relatively constant mean cluster radius over about 30 s, indicates that cluster nucleation predominates during this period. Subsequently, a decrease in cluster density and an increase in mean cluster radius suggest that Cu cluster growth dominates the evolution in this regime.

Ferritic and ferritic/martensitic steels are considered for next-generation IV or fusion nuclear reactors. Under low-temperature conditions, the iron-rich phase (α) and the chromium-rich phase (α') undergo co-phase separation, leading to mechanical property degradation. Irradiation can drastically accelerate this phase transition by generating excess point defects. Simultaneously, irradiation causes ballistic mixing between alloy components within the displacement cascade, hindering precipitation formation or reducing precipitation size.[30] This phenomenon may elucidate the absence of α' precipitation during ion irradiation at very high dose rates.[82] To obtain the impact of a high dose rate on α' precipitation, Soisson et al.[70] utilized the CD method to simulate the kinetic process of α' precipitation in the Fe−15%Cr alloy under diverse irradiation conditions and obtained the precipitation mean radius and density. The model incorporated key mechanisms influencing precipitation kinetics, including vacancies and interstitials formation and their elimination on defect sinks. In neutron irradiation, interstitial and vacancy clusters introduced by intra-cascades were considered, revealing precipitates with a radius of approximately 1.2 nm, consistent with existing experiments. For electron irradiation, the generated term G_n encompassed only mono-interstitials and vacancies. Electron irradiation, characterized by a higher dose rate, resulted in elevated point defect concentrations and displayed a classical nucleation growth stage for α' precipitation. The obtained average radius of α'

precipitation closely matched the experimental observations, with no discernible reduction concerning precipitation size and number density. Hence, the CD model revealed that ballistic mixing has a minimal impact on the chromium-rich phase precipitates in Fe−15%Cr alloy.

Incorporating transition elements such as Zr or Sc into Al alloys promotes the formation of small precipitation, reducing the alloy sensitivity to recrystallization. Clouet et al.[83] studied the precipitation of Sc in an Al-Sc alloy under various temperature conditions. The CD model accurately reproduced the variation of the mean precipitate radius with time and the precipitation size distribution, as depicted in Fig. 9c and d in the Al-Sc alloy. It revealed the effect of temperature on accelerating cluster growth observed in experiments due to higher absorption rates at elevated temperatures. Guyot et al.[84] suggested that nucleation and cluster growth in the CD model are governed by defect diffusivities. By adjusting the content of Zr and Sc to modify the diffusion coefficient in the CD model, simulation results revealed that, in the Al3(Zr, Sc) alloy, the fast-diffusing species (Sc) aided in nucleation, while the slow-diffusing solute (Zr) slowed their growth rate.

The simulations demonstrate that, by choosing suitable parameters like the diffusion coefficient of precipitation and the precipitation free energy associated with interface energy, the CD model can effectively simulate nucleation and growth of precipitation. In addition, the precipitate size is intricately linked to the type of irradiation source, irradiation temperature, and material composition.

Irradiation-Induced Swelling

Irradiation-induced swelling, attributed to the growth of vacancy clusters and bubbles, has been extensively studied using CD models across various materials, including metallic alloys[85] and ceramic fuels.[86,87] To investigate the effect of defect reaction rate on gas bubble swelling in irradiated polycrystalline UMo fuel, Hu et al.[88] employed CD models to simulate defect accumulation and gas bubble growth. The CD model considered only single interstitials, vacancies, and gas atoms as mobile, accounting for defect generation, diffusion, reaction between defects, and absorption by sinks. Simulation results revealed that swelling induced by bubble size increases with defect generation and absorption rates but decreased with an increase in the defect sink rate at grain boundaries. Dunn et al.[89] examined the impact of grain size on vacancy cluster growth using the CD model in α-Fe. The model accounted for the diffusion and reaction of single vacancies, interstitials, and corresponding clusters. Grain boundaries were treated as perfect sinks for mobile defects. Additionally, the model incorporated the one-dimensional movement of dislocation loops larger than 4 interstitials. Figure 10a and b illustrates the population of vacancy clusters inside the grains, indicating that increasing the number of grains decreases vacancy cluster concentration and average size, consistent with experimental trends. Du et al.[90] utilized the CD model to explore the effect of grain size on swelling in nanocrystalline stainless steel containing 1 at.% lanthanum. The model accounted for the clustering of interstitials and vacancies, with grain boundaries and dislocations considered as sink sites of defects. Figure 10c depicts the distribution of vacancy concentrations at steady state, while Fig. 10d demonstrates the average vacancy and interstitial concentrations with different average grain sizes. The CD model reveals that the concentration of interstitials is much smaller than that of vacancies due to their higher mobility, making them easier to be captured by grain boundaries. In addition, as the average grain size diminishes, the concentrations of both interstitials and vacancies decrease. The CD model emphasizes the inhibition of cluster growth in nanocrystalline materials, resulting in negligible void swelling.

CHALLENGES AND OPPORTUNITIES OF CD IN IRRADIATION DAMAGE

The evolution of defects during irradiation is governed by various factors, including the defect generation rate, the mobility and diffusivity of clusters, and the binding properties of clusters. The defect production rate, influenced by the forms of produced defects (Frenkel pair or intra-cascade clusters) and flux, dictates the distribution of initial defects for the subsequent evolution of defects. Cluster mobility, determined by parameters such as prefactor (D_0) and migration energy (E_m), impacts the absorption and emission dynamics. The binding/free energy reflects the thermal stability of the clusters and dictates their emission rate. While CD simulations are commonly employed for studying the evolution of irradiation-induced defects, it is crucial to consider several limitations when applying CD models.

(1) The effect of uncertainty in model parameters on cluster evolution. Even in the simplest CD model, defect evolution entails more than a dozen parameters. Uncertainties in these parameters can profoundly affect the results obtained from simulations. For instance, each cluster necessitates several parameters to comprehensively describe the reaction rates, which are influenced by factors such as cluster morphology, composition, mobility, and interaction radius. Consequently, there is a pressing requirement to establish a precise database of fundamental properties of clusters with varying sizes in the materials under consideration. However, such a database is relatively difficult due to the spatial scales involved. Ab initio calculations are impractical

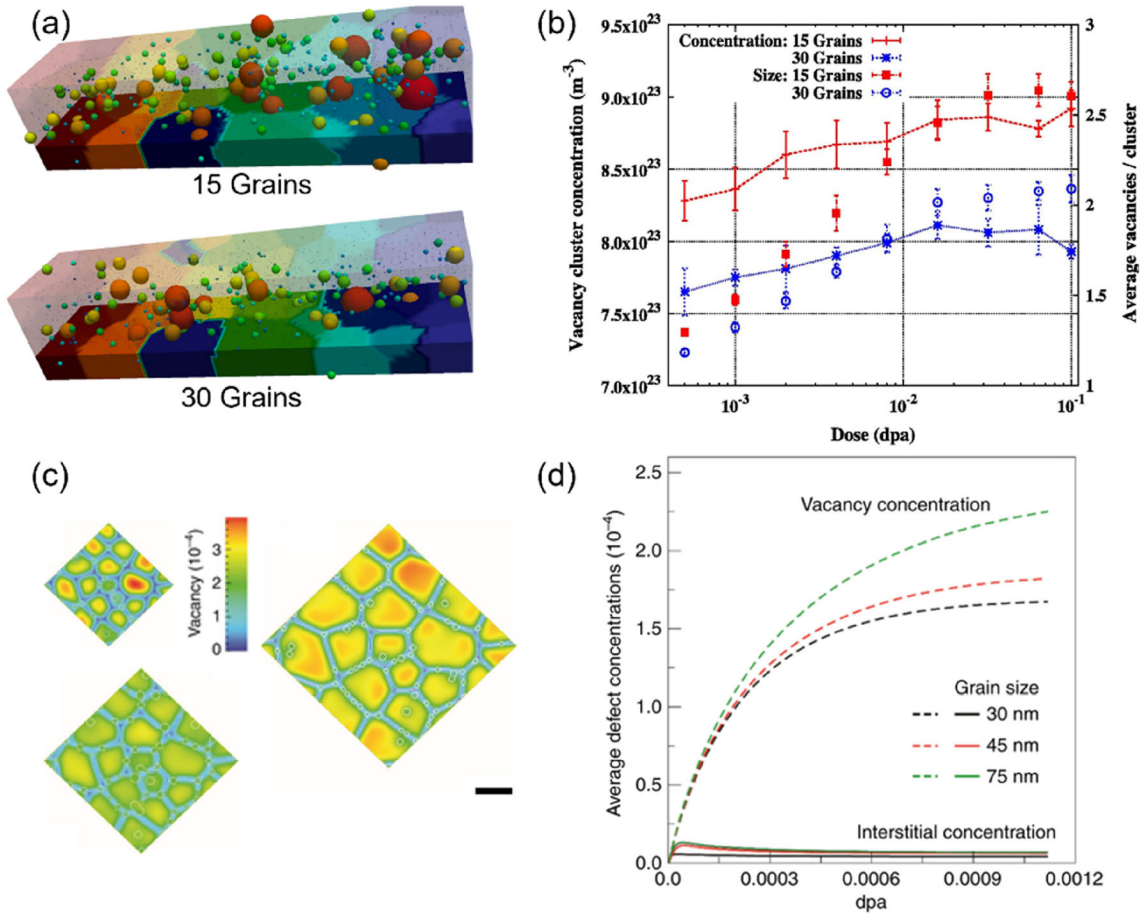

Fig. 10. (a) Visualization of grain structure and vacancy cluster (spheres) distribution in simulated polycrystals. (b) Vacancy cluster concentration and their averaged size as a function of dose. (c) Distributions of vacancy concentrations in the nanocrystalline stainless steel. (d) The effect of grain size on the evolution of averaged interstitial and vacancy concentrations. (a, b) Reprinted with permission from Ref. 89; (c, d) reprinted with permission from Ref. 90 under Creative Commons License CC-BY.

as large defect clusters need to be considered. MD approaches may be pursued but are subject to the availability and accuracy of interatomic potentials.

(2) The effect of heterogeneity in materials. Parameters governing cluster behavior can exhibit strong space correlation and inhomogeneity within a given material, particularly in HEAs. Specifying the spatial variations of these parameters is exceedingly complex and can greatly augment the intricacy of the CD model. Moreover, acquiring such detailed information can be challenging. During irradiation, elemental segregation around dislocation loops may promote heterogeneous elemental distribution, thereby altering the rate constants of clusters. Additionally, neutron irradiation can induce the transmutation of elements in materials (e.g., Re and Os in W), leading to changes in fundamental cluster properties and consequently impacting cluster evolution. Indeed, effectively considering spatial correlation or making reasonable approximations is an area worthy of further exploration. One approach could incorporate statistical methods or machine learning techniques to capture spatial correlations in material properties and defect evolution. Note that machine learning models have been actively developed currently to model the spatial characteristics and correlations of defects in HEAs, although they are still restricted to point defects.[91–94]

CONCLUSION

This review has mainly focused on the establishment of the master equation in the CD simulation and discusses the influence of cluster mobility, intra-cascade cluster formation, materials composition, temperature, and irradiation conditions on cluster size distributions. We then introduced the applications of CD models in modeling irradiation-induced effects in nuclear materials, including radiation-induced defect nucleation and growth, precipitations, and swelling. In general, CD models provide a critical theoretical approach for studying the radiation damage mechanism of reactor

materials, and the relevant simulation results can guide the development and design of irradiation-resistant nuclear materials. In the future development of CD simulations, more sophisticated physics processes such as heterogeneity and transmutation should be more rigorously incorporated. Establishing an accurate database of basic properties of clusters with different sizes rather than empirical fit is vital to the analysis of the defect nucleation and growth. Finally, to obtain accurate solutions of cluster size distribution at high doses, the application of artificial intelligence in solving a large number of partial differential equations is also expected, whereas traditional accurate solutions often consume a lot of time and computing resources. Overall, interdisciplinary research efforts combining materials science, statistics, and computational modeling are essential for advancing our understanding of material and defect behavior.

ACKNOWLEDGEMENTS

This work was supported by the National Key R&D Program of China (No. 2022YFE0200900) and the Shenzhen Basic Research Program (JCYJ20230807114959029).

CONFLICT OF INTEREST

On behalf of all authors, the corresponding author states that there is no conflict of interest.

REFERENCES

1. S.J. Zinkle and G.S. Was, *Acta Mater.* 61(3), 735 (2013).
2. E.A. Kenik and J.T. Busby, *Mater. Sci. Eng. R. Rep.* 73(7), 67 (2012).
3. X. Zhang, K. Hattar, Y. Chen, L. Shao, J. Li, C. Sun, K. Yu, N. Li, M.L. Taheri, H. Wang, et al., *Prog. Mater. Sci.* 96, 217 (2018).
4. G. Ackland, *Science* 327(5973), 1587 (2010).
5. C.P. Race, D.R. Mason, M.W. Finnis, W.M.C. Foulkes, A.P. Horsfield, and A.P. Sutton, *Rep. Prog. Phys.* 73(11), 116501 (2010).
6. S. Ma, W. Liu, Q. Li, J. Zhang, S. Huang, Y. Xiong, B. Xu, T. Yang, and S. Zhao, *Acta Mater.* 264, 119537 (2024).
7. T. Diaz de la Rubia, H.M. Zbib, T.A. Khraishi, B.D. Wirth, M. Victoria, and M.J. Caturla, *Nature* 406(6798), 871 (2000).
8. C.-C. Fu, J.D. Torre, F. Willaime, J.-L. Bocquet, and A. Barbu, *Nat. Mater.* 4(1), 68 (2005).
9. D.J. Bacon, and Y.N. Osetsky, *Int. Mater. Rev.* 47(5), 233 (2002).
10. G.R. Odette, B.D. Wirth, D.J. Bacon, and N.M. Ghoniem, *MRS Bull.* 26(3), 176 (2001).
11. S.K. Mazumder, T. Yao, and A. El-Azab, *Acta Mater.* 8(24), 119728 (2024).
12. S.K. Mazumder, K. Bawane, J.M. Mann, A. French, L. Shao, L. He, and A. El-Azab, *J. Nucl. Mater.* 586, 154686 (2023).
13. A. Roy, M. Sassi, K.C. Pitike, M.S. Lanza, A.M. Casella, D.J. Senor, C. Matthews, D.A. Andersson, and R. Devanathan, *J. Nucl. Mater.* 592, 154970 (2024).
14. S. Cui, *Metall. Mater. Trans. A.* 024, 07357 (2024).
15. S. Zhao, Y. Xiong, S. Ma, J. Zhang, B. Xu, and J.-J. Kai, *Acta Mater.* 219, 117233 (2021).
16. S. Huang, J. Zhang, Y. Xiong, S. Ma, B. Xu, and S. Zhao, *J. Nucl. Mater.* 568, 153877 (2022).
17. J. Gao, E. Gaganidze, and J. Aktaa, *Acta Mater.* 233, 117983 (2022).
18. A.V. Barashev, Q. Zhao, Q. Wang, Q. Yan, and F. Gao, *J. Nucl. Mater.* 561, 153521 (2022).
19. M. Mamivand, P. Wells, H.B. Ke, S.P. Shu, G.R. Odette, and D. Morgan, *Acta Mater.* 180, 199 (2019).
20. T. Stegmuller, and F. Haider, *Acta Mater.* 177, 240 (2019).
21. T.L. Hoang, R. Nazarov, C. Kang, and J.Y. Fan, *Nucl. Instrum. Methods Phys. Res. Sect. B-Beam Interact. Mater. Atoms* 427, 9 (2018).
22. K.D. Hammond, S. Blondel, L. Hu, D. Maroudas, and B.D. Wirth,*Acta Mater.* 144, 561 (2018).
23. A.A. Kohnert, B.D. Wirth, and L. Capolungo, *Comput. Mater. Sci.* 149, 442 (2018).
24. D. Chen, X. He, G. Chu, X. He, L. Jia, Z. Wang, W. Yang, and C. Hu, *SIMULATION* 97(10), 659 (2021).
25. Q. Zheng, L. Wei, and Y. Li, C. Zhang, and Z. Zeng, *Atom. Energy Sci. Technol.* 55(1), 76 (2021).
26. J.-H. Ke, *Comput. Mater. Sci.* 230, 112503 (2023).
27. H.B. Ke, P. Wells, P.D. Edmondson, N. Almirall, L. Barnard, G.R. Odette, and D. Morgan, *Acta Mater.* 138, 10 (2017).
28. J.H. Ke, E.R. Reese, E.A. Marquis, G.R. Odette, and D. Morgan, *Acta Mater.* 164, 586 (2019).
29. M. Mamivand, Y. Yang, J. Busby, and D. Morgan, *Acta Mater.* 130, 94 (2017).
30. F. Soisson, and T. Jourdan, *Acta Mater.* 103, 870 (2016).
31. B. Cheng, W.T. Wan, G.Y. Huang, Y.H. Li, G.M. Genin, M.R.K. Mofrad, T.J. Lu, F. Xu, and M. Lin, *Sci. Adv.* 6(10), 2375 (2020).
32. J.H. Ke, H.B. Ke, G.R. Odette, and D. Morgan, *J. Nucl. Mater.* 498, 83 (2018).
33. C. Liu, L. He, Y. Zhai, B. Tyburska-Puschel, P.M. Voyles, K. Sridharan, D. Morgan, and I. Szlufarska, *Acta Mater.* 125, 377 (2017).
34. S. Pellegrino, J.-P. Crocombette, A. Debelle, T. Jourdan, P. Trocellier, and L. Thomé, *Acta Mater.* 102, 79 (2016).
35. Y. Katoh, N. Hashimoto, S. Kondo, L.L. Snead, and A. Kohyama, *J. Nucl. Mater.* 351(1), 228 (2006).
36. T. Jourdan, G. Bencteux, and G. Adjanor, *J. Nucl. Mater.* 444(1), 298–313 (2014).
37. A.A. Kohnert, and B.D. Wirth, *J. Appl. Phys.* 117(15), 154306 (2015).
38. V.V. Slezov, *Phase Transit.* 429, 7 (2009).
39. J. Marian, and V.V. Bulatov, *J. Nucl. Mater.* 415(1), 84 (2011).
40. M.F. Wehner, and W. Wolfer, *Phys. Rev. A* 27(5), 2663 (1983).
41. M.P. Surh, J. Sturgeon, and W. Wolfer, *J. Nucl. Mater.* 328(2–3), 107 (2004).
42. M.P. Surh, J. Sturgeon, and W. Wolfer, *J. Nucl. Mater.* 325(1), 44 (2004).
43. M.P. Surh, J.B. Sturgeon, and W.G. Wolfer, *J. Nucl. Mater.* 378(1), 86 (2008).
44. S. Golubov, A. Ovcharenko, A. Barashev, and B. Singh, *Philos. Mag. A* 81(3), 643 (2001).
45. A.A. Kohnert, and B.D. Wirth, *Modell. Simul. Mater. Sci. Eng.* 25(1), 015008 (2016).
46. D. Xu, and B.D. Wirth, *J. Nucl. Mater.* 403(1), 184 (2010).
47. A.Y. Dunn, M.G. McPhie, L. Capolungo, E. Martinez, and M. Cherkaoui, *J. Nucl. Mater.* 435(1), 141 (2013).
48. A.Y. Dunn, L. Capolungo, E. Martinez, and M. Cherkaoui, *J. Nucl. Mater.* 443(1–3), 128 (2013).
49. A. Dunn, L. Capolungo, *Comput. Mater. Sci.* 102, 314 (2015).
50. M.L. Jenkins, M.A. Kirk, *Characterisation of radiation damage by transmission electron microscopy* 11, 224 (2000).
51. D. Xu, B.D. Wirth, M. Li, and M.A. Kirk, *Acta Mater.* 60(10), 4286 (2012).
52. S. Cui, M. Mamivand, and D. Morgan, *Mater. Des.* 191, 108574 (2020).
53. E. Meslin, A. Barbu, L. Boulanger, B. Radiguet, P. Pareige, K. Arakawa, and C.C. Fu, *J. Nucl. Mater.* 382(2), 190 (2008).
54. T. Jourdan, and J.P. Crocombette, *Comput. Mater. Sci.* 145, 235 (2018).

55. E. Meslin, B. Radiguet, and M. Loyer-Prost, *Acta Mater.* 61(16), 6246 (2013).
56. Y. Xiong, J. Zhang, S. Ma, S. Huang, B. Xu, and S. Zhao, *J. Alloy. Compd.* 953, 170084 (2023).
57. Y. Xiong, J. Zhang, S. Ma, B. Xu, and S. Zhao, *Mater. Des.* 225, 111573 (2023).
58. J. Xue, S. Jin, R. Hu, F. Xue, and G. Sha, *J. Nucl. Mater.* 560, 153477 (2022).
59. S.A. Briggs, C.M. Barr, J. Pakarinen, M. Mamivand, K. Hattar, D.D. Morgan, M. Taheri, and K. Sridharan, *J. Nucl. Mater.* 479, 48 (2016).
60. D. Brimbal, L. Fournier, and A. Barbu, *J. Nucl. Mater.* 468, 124 (2016).
61. Y. Li and N. Ghoniem, *J. Nucl. Mater.* 540, 152312 (2020).
62. H. Bai, C. Hu, Y. Zhu, and D. Chen, *Nucl. Eng. Des.* 415, 112633 (2023).
63. F. Granberg, K. Nordlund, M.W. Ullah, K. Jin, C. Lu, H. Bei, L. Wang, F. Djurabekova, W. Weber, and Y. Zhang, *Phys. Rev. Lett.* 116(13), 135504 (2016).
64. X. Yi, M.L. Jenkins, K. Hattar, P.D. Edmondson, and S.G. Roberts, *Acta Mater.* 92, 163 (2015).
65. Q. Dong, H. Qin, Z. Yao, and M.R. Daymond,*Mater. Des.* 161, 147 (2019).
66. X.M. Bai, H.B. Ke, Y.F. Zhang, and B.W. Spencer, *J. Nucl. Mater.* 495, 442 (2017).
67. J.C. Haley, S. de Moraes Shubeita, P. Wady, A.J. London, G.R. Odette, S. Lozano-Perez, and S.G. Roberts, *J. Nucl. Mater.* 533, 152130 (2020).
68. E.R. Reese, N. Almirall, T. Yamamoto, S. Tumey, G. Robert Odette, and E.A. Marquis, *Scripta Mater.* 146, 213 (2018).
69. A. Gokhman, and F. Bergner, *Radiat. Eff. Defects Solids* 165(3), 216 (2010).
70. F. Soisson, E. Meslin, and O. Tissot, *J. Nucl. Mater.* 508, 583 (2018).
71. Y.G. Li, W.H. Zhou, L.F. Huang, Z. Zeng, and X. Ju, *J. Nucl. Mater.* 431(1), 26 (2012).
72. A. Dunn, R. Dingreville, E. Martínez, and L. Capolungo, *Acta Mater.* 110, 306 (2016).
73. A. Dunn, B. Muntifering, R. Dingreville, K. Hattar, and L. Capolungo, *J. Nucl. Mater.* 480, 129 (2016).
74. F. Christien, and A. Barbu, *J. Nucl. Mater.* 393(1), 153 (2009).
75. J. Zhang, S. Ding, and H. Duan, *J. Nucl. Mater.* 577, 154295 (2023).
76. F. Christien, and A. Barbu, *J. Nucl. Mater.* 346(2), 272 (2005).
77. C. Matthews, R. Perriot, M.W.D. Cooper, C.R. Stanek, and D.A. Andersson, *J. Nucl. Mater.* 540, 152326 (2020).
78. A. Debelle, J.-P. Crocombette, A. Boulle, E. Martinez, B.P. Uberuaga, D. Bachiller-Perea, Y. Haddad, F. Garrido, L. Thomé, and M. Béhar, *Phys. Rev. Mater.* 2(8), 083605 (2018).
79. A. Debelle, J.-P. Crocombette, A. Boulle, A. Chartier, T. Jourdan, S. Pellegrino, D. Bachiller-Perea, D. Carpentier, J. Channagiri, T.-H. Nguyen, et al., *Phys. Rev. Mater.* 2(1), 013604 (2018).
80. T. Jourdan, F. Soisson, E. Clouet, and A. Barbu, *Acta Mater.* 58(9), 3400 (2010).
81. M. Mathon, A. Barbu, F. Dunstetter, F. Maury, N. Lorenzelli, and C. De Novion, *J. Nucl. Mater.* 245(2–3), 224 (1997).
82. C. Pareige, V. Kuksenko, and P. Pareige, *J. Nucl. Mater.* 456, 471 (2015).
83. E. Clouet, A. Barbu, L. Laé, and G. Martin, *Acta Mater.* 53(8), 2313 (2005).
84. P. Guyot, J. Lepinoux, and C. Sigli, *Int. J. Mater. Res.* 100(10), 1440 (2009).
85. Z. Zhao, Y. Li, C. Zhang, G. Pan, P. Tang, and Z. Zeng, *Nucl. Fus.* 57(8), 086020 (2017).
86. D. Pizzocri, G. Pastore, T. Barani, A. Magni, L. Luzzi, P. Van Uffelen, S.A. Pitts, A. Alfonsi, and J.D. Hales, *J. Nucl. Mater.* 502, 323 (2018).
87. G. Pastore, N. Militello, S. Blondel, and B.D. Wirth, *J. Nucl. Mater.* 583, 154453 (2023).
88. S. Hu, W. Setyawan, B.W. Beeler, J. Gan, and D.E. Burkes, *J. Nucl. Mater.* 542, 152441 (2020).
89. A. Dunn, R. Dingreville, E. Martinez, and L. Capolungo, *Comput. Mater. Sci.* 120, 43–52 (2016).
90. C. Du, S. Jin, Y. Fang, J. Li, S. Hu, T. Yang, Y. Zhang, J. Huang, G. Sha, Y. Wang, et al., *Nat. Commun.* 9(1), 5389 (2018).
91. B. Xu, J. Zhang, Y. Xiong, S. Ma, Y. Osetsky, and S. Zhao, *Cell Rep. Phys. Sci.* 4(4), 101337 (2023).
92. B. Xu, S. Ma, S. Huang, J. Zhang, Y. Xiong, H. Fu, X. Xiang, and S. Zhao, *Phys. Rev. Mater.* 7(3), 033605 (2023).
93. B. Xu, S. Ma, Y. Xiong, J. Zhang, S. Huang, J.-J. Kai, and S. Zhao, *Mater. Des.* 223, 111238 (2022).
94. B. Xu, J. Zhang, S. Ma, Y. Xiong, S. Huang, J.J. Kai, and S. Zhao, *Acta Mater.* 234, 118051 (2022).